A stereo optical comparison method for detection of metallic surface defects based on machine vision and laser triangulation

Heng Li*, *Amir A* Mokhtarzadeh, *Guohao* Li, and *Hong* Zhou

Huaiyin Institute of Technology, Faculty of Computer and Software Engineering, 223003, 1, Meicheng East Road, Huaian, Jiangsu, China

Abstract. Quality of metallic surfaces is essential to maintain performance and longevity of industrial products. The surface defects of products like holes and cracks not only affect their appearances and performance, but also may even result in potential danger to human health in some cases. Traditional surface inspection methods for metallic surfaces rely on manual inspection methods by naked eyes or with the help of close circuit cameras, presenting the problems of low efficiency, low accuracy, high labour intensity due to monotonous work. Today manual inspection is not possible in many applications, therefore an automated method with a high accuracy is desirable. In this paper we propose a novel stereo optical comparison method to detect defects on metallic surface based on machine vision and laser triangulation.

1 Introduction

Quality of metallic surfaces like steel or aluminum is essential to maintain performance and longevity of industrial products, surface defects of products like holes, pits, cracks or scratches affect their appearances, degrades their performances, and even cause accidents.

The proposed method in this paper is a stereo optical comparison method based on machine vision and laser triangulation to detect the defects on metallic surfaces.

In recent years, quantity of research on surface defects based on laser triangulation or image processing have been conducted in different fields of production industries like metal, fabric, tiling, glass, etc [1]. Chengxing Wu [2] developed a method using a differential laser triangulation to detect defects on corrugated plate surfaces, this method adopted a pair of laser triangulation probes to acquire data of the examined plate. A novel algorithm based on image pyramid and image reconstruction to detect surface defects in friction stir welding is proposed in [3], by which vertical intensity plot and the area plot of the defect blobs could be represented, and then surface defect in welding like voids, grooves and cracks can be identified and located. In [4], a method using Canny edge and histogram analysis was developed for surface finish and defect inspection in a grinding process, according to the edge patterns and gray level distribution derived from original images, different gray scale distribution represented different kind of surfaces, hence smooth, rough or defective surface

* Corresponding author: 1363467258@qq.com

can be identified and classified. [5] proposed an approach based on image processing to evaluate surface detects of yarn, the images were converted into binary format by Otsu's method, after removing the noise, detects area was determined by the number of pixels and the region.

2 Methodology

Laser triangulation is one important method in the field of machine vision, which has simple structure and high cost-effect, it also has the advantages of non-contact and fast response, given these virtues, laser triangulation is always used for displacement calculation, position measurement and aperture measurement of mechanical parts, 3D modeling and surface characteristics capture such as cracks, gaps, roughness, etc.

The rationale of laser triangulation is shown in Fig.1: A laser beam emitted by the laser diode is collimated to the point M on the surface of the object to be measured through the focusing lens in normal incidence. At this time, the angle between the incident light and the normal of the object surface is 0 degree, and the angle between the reflected light and the normal of the object surface is β, the reflected light is imaged at the M' point of the CCD, while the angle between the light and the CCD image plane is γ. When the object moves to point N, the imaging point of the incident beam moves to the point N' of the CCD [6].

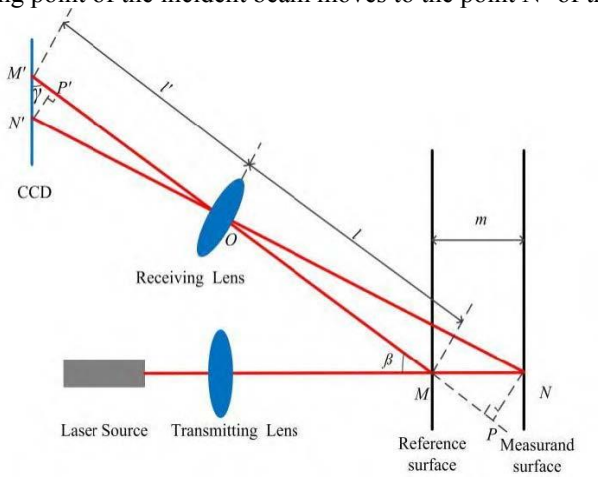

Fig. 1. Rationale of laser triangulation method [6].

According to the principle of similar triangle, we can get formula like:

$$\frac{NP}{OP}=\frac{N'P'}{OP'} \tag{1}$$

Then formula (1) can be rewritten as follows according to the relationship of edges of angles in Fig.1:

$$\frac{m\sin\beta}{l+m\cos\beta}=\frac{M'N'\sin\gamma}{\frac{fl}{1-f}-M'N'\cos\gamma} \tag{2}$$

So, distance or displacement m can be expressed as following:

$$m = \frac{(1-f)M'N'\sin\gamma}{f\sin\beta - M'N'(1-\frac{f}{l})\sin(\beta+\gamma)} \tag{3}$$

where l and f represent object distance and focal length of the receiving lens respectively.

However, the precision of laser triangulation is prone to be influenced by the laser jitter, the color of the object surface to be measured, the detection accuracy of laser spot, therefore, stereo cameras positioned at opposite angles are utilized to alleviate this problem.

Therefore a series of image processing procedures is essential to separate optical noises before employing laser triangulation measurement.

Color image obtained in practical application always need to be translate to grayscale image for subsequent processing, then Gaussian blur is applied to the grayscale image for denoising. Gaussian blur can retain more of the overall gray distribution characteristics of the image while obtaining a superior blur effect, making it perform better compared with other blur methods. The Gaussian distribution in 2-dimensional space can be expressed by:

$$G(x,y) = \frac{1}{2\pi\sigma^2}\exp(-\frac{x^2+y^2}{2\sigma^2}) \tag{4}$$

where σ stands for the standard deviation of the Gaussian distribution, and (x,y) represents the coordinate of element on the Gaussian template. After Gaussian blur, the whole image will present a blurred vision effect, some details we don't care about and some noise we don't want to see are eliminated, which is conducive to the next processing.

The selection of the threshold plays a decisive role in the binarization result. Otsu is the optimal algorithm to decide the thresholding value in most of practical applications [7], which is also known as maximization of interclass variance algorithm. Formulae (5) - (7) show the principle of Otsu algorithm:

$$m = m_0 p_0 + m_1 p_1 \quad \text{s.t.} \quad p_0 + p_1 = 1 \tag{5}$$

$$g = p_0(m_0 - m)^2 + p_1(m_1 - m)^2 \tag{6}$$

$$g = p_0 p_1 (m_0 - m_1)^2 \tag{7}$$

where m_0, p_0, m_1, p_1 represent the average pixel value of foreground, the proportion of foreground pixels, the average pixel value of background, the proportion of background pixels respectively, m stands for the average value of the whole image, and g stands for the interclass variance, the whole image is traversed to get all the possible threshold T, trying to get the maximum value of g, then the threshold will be determined while g reach to the maximum value.

After image binarization, morphological image processing is exploited for further handling. Morphological processing can extract Regions of Interest (ROI) or implement other relevant image manipulations that are desired with a set of a known pattern called structure element [8]. Canny algorithm [9] is a recognized outstanding algorithm for edge detection in the image processing fields since it was first proposed in 1986. The steps of Canny algorithm could be concluded as follows:

(1) Utilize Gaussian filter aforementioned to smooth input image.

(2) The gradient amplitude and direction are calculated to estimate the edge strength and direction at each point:

$$M_s(x,y) = \| \nabla f_s(x,y) \| = \sqrt{g_x^2(x,y) + g_y^2(x,y)} \quad (8)$$

$$\alpha(x,y) = \arctan\left(\frac{g_y(x,y)}{g_x(x,y)}\right) \quad (9)$$

where $f_s(x,y)$ is the result of Gaussian smoothing, while $g_x(x,y)$ and $g_y(x,y)$ stand for partial derivation of $f_s(x,y)$ to x and y.

(3) The gradient amplitudes derived from (2) is suppressed to sharp the edges, the pixels that turn out to be maximal in this comparison are marked with white borders, whilst other pixels will be suppressed.

(4) Double-thresholding policy is adopted to screen the edges acquired from non-maximum suppression, Edge pixels stronger than the high threshold are marked as strong; edge pixels weaker than the low threshold are suppressed and edge pixels between the two thresholds are marked as weak.

In order to extract features from the image, contours are employed. Contours can be expressed as a curvilinear border conjoining all the continuous points (along the boundaries or edges) with same color or intensity.

3 Experimental system and result

The experiments are conducted in our Robotics Research lab by especially developing an automated laser scanning device equipped with stereo cameras, SBC (Single Board Computer) and all necessary support hardware and software. The scanning head can be programmed to receive starting point A, end point B and start scanning with a given speed. The whole process is controlled from the main surface defect software. At each programmable interval during scanning, the main software takes a quick measurement and check for integrity of the laser line.

3.1 Model and hardware device of experimental system

Our model of stereo optical comparison surface defect detection is demonstrated by Fig.2:

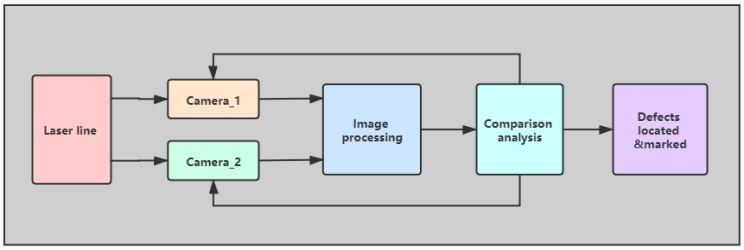

Fig. 2. Stereo optical comparison model of process of each defect detection.

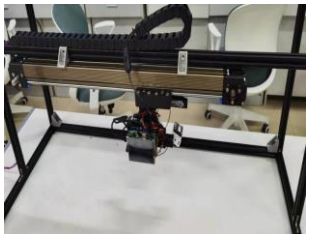

Fig. 3. X-Y axial frame of experimental system.

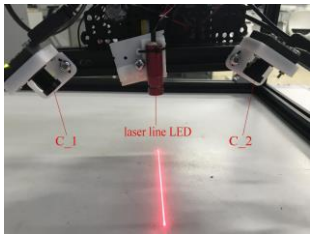

Fig. 4. Stereo comparison detection device.

Our exprimental sysetem system was built under a X-Y axial frame shown in Fig.3, and stereo comparison detection device was constructed with two cameras (labelled as C_1 and C-2 respectively) pisitioned on the left and right sides of the laser LED shown in Fig.4

By using Raspberry Pi as the main processing SBC (Single Board Computer), and CMOS cameras, at each given step an image is taken by two cameras, automatically cut at ROI selection and tested for any distortion on the laser line. This process is fairly quick. However, if any distortion detected, images are saved for further analysis.

3.2 Detection of surface integrity

Scanning process can be viewed from only one camera for purpose of monitoring the operation (Fig. 5)

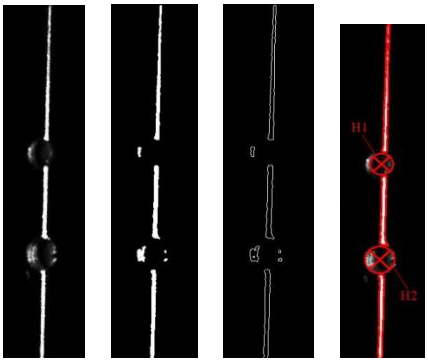

(a) (b) (c) (d)

Fig. 5. Image processing for laser line.

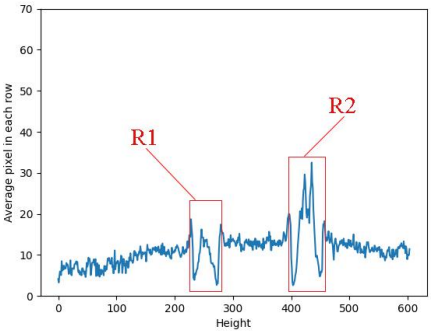

Fig.6. Specialized histogram of ROI of original image.

In Fig.5, (a), (b), (c) and (d) represent ROI of original image from video stream, image after morphological opening operation on (a), Canny edge detection on (b), holes located and marked in the image respectively.

During scanning process, images will be taken from suspected areas for further investigation. The first process will inspect any defects larger than 0.5 mm in dept, or in width. The second process will check for cracks larger than 0.5 mm. These sizes and dimensions particularly depend on the application and they are adjustable. However, devices we have used for our experiments are capable of detecting a hole or crack larger than 0.5 mm with 0.02 mm percision.

The process of detection of the defect starts with a Gaussian filter to blur the original image. the larger the size of Gaussian kernel is, the more obvious the blurring effect is, binarization using Otsu algorithm and morphological opening operation will be applied to the blurred image, and the resultant image is shown in Fig.5.(b).

Even though it's not obvious enough, compared to the original image, some tiny noise is removed after morphological opening operation, and the laser lines in the resultant image present a sharper and thicker visual effect than those in the original image. In the next step, Canny algorithm is exploited to detect the edges in the image. The detection result is show as following in Fig.5.(c).

Subsequently, contours was searched according to the detected edges, the desired contours are contours of laser lines which we need to use to calculate the position of holes, however there are always unexpected contours existing, hence, bounding rectangles surrounding the contours was calculated, then according the information of bounding rectangles, contours don’t satisfy the requirement of height and width will be excluded in

the process of calculation, the holes of the surface are located and marked in red circular cross symbol as Fig.5.(d) shows.

Here we introduce a specialized histogram monitoring the pixel change through the laser line. The histogram of ROI of original image (Fig.5.(a)) is depicted by Fig.6.

The abscissa of histogram represents the height of the image, and the ordinate represents the average pixel value of each row of the image. From the histogram, we can notice that there exist two regions with sharp change in pixel values, which named as R1 and R2 respectively, corresponding to two holes marked as H1 and H2 in Fig.5.(d) respectively, and the fluctuation of other regions in this histogram is relatively gentle, corresponding to non-defective part of laser line detection in Fig.5. (d).

As can be seen in Fig.4, two cameras (C_1 and C_2) can obtain two images of same position on the surface but under different condition of illumination and reflection because of the different positions of cameras, the single camera's detection result could be rectified by two cameras' comparison.

Examples of two cameras' stereo comparison detection are shown in Fig.7 and Fig.9. Fig.7 shows the different detection results of both two cameras, while Fig.11 shows same detection results from these two cameras after adjusting position and angle of C_2.

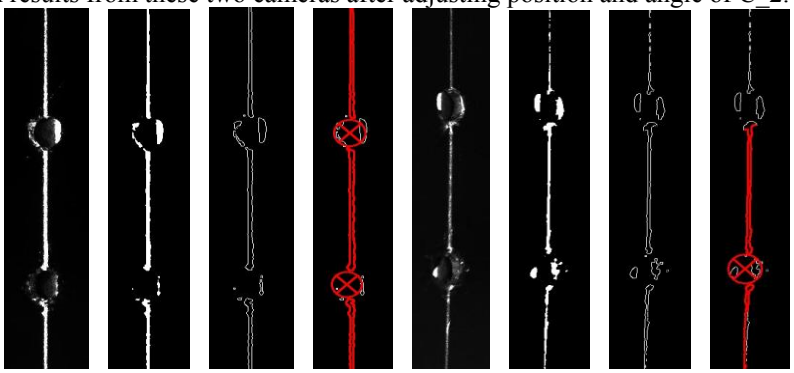

Fig. 7. Example of different detection results of two cameras.

In Fig.7, (a), (b), (c), (d) represent gray scale image of laser line captured by C_1, binarization and morphological operation on (a), Canny edge on (b), contours found on (c) and defects detected with mark respectively, while (e), (f), (g), (h) stand for gray scale image of laser line captured by C_2, binarization and morphological operation on (e), Canny edge on (f), contours found on (g) and defects detected with mark respectively.

Histogram of gray scale images captured by two cameras (i.e. Fig.7. (a) and Fig.7. (e)) are calculated shown in Fig.8.

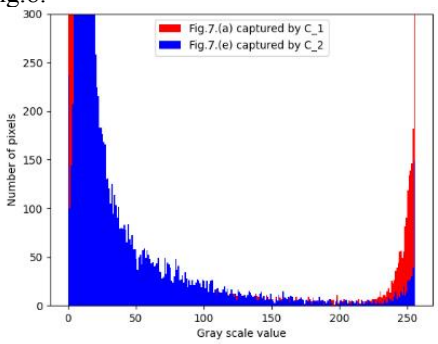

Fig. 8. Histogram of Fig.7.(a) and Fig.7.(e).

To reduce the loss of details in image captured by C_2, distance and angle of C_2 from laser line LED are adjusted by servo motor to conduct another experiment as shown in Fig.9.

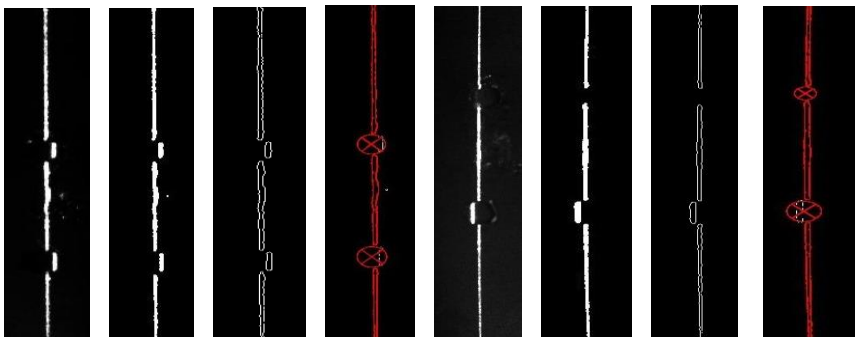

Fig. 9. Same detection results of two stereo cameras after adjusting position and angle of C_2.

The graphs in Fig.9 and Fig.10 demonstrate the advantage of stereo cameras to reduce illumination and reflection disadvantages. In Fig.9, (a), (b), (c), (d) represent gray scale image of laser line captured by C_1, binarization and morphological operation on (a), Canny edge on (b), contours found on (c) and defects detected with mark respectively, while (e), (f), (g), (h) stand for gray scale image of laser line captured by C_2, binarization and morphological operation on (e), Canny edge on (f), contours found on (g) and defects detected with mark respectively.

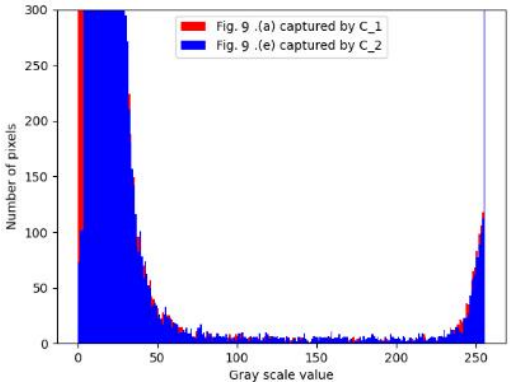

Fig. 10. Histograms of Fig.9. (a) and Fig.9. (e).

Similarly, histograms of Fig.9.(a) and Fig.9.(e) are compared in Fig.10, between these two histograms, they show great similarity, which is the decisive factor for stereo cameras to get same detection results, while within each histogram, it shows obvious pixel differences, contributing to correct detection.

To calculate the size of defects such as hole or gap in cracks, we will refer to laser triangulation method for laser line with known distance between camera and the surface shown in Fig.11.

3.3 Detection of curving surface

When a laser line is reflected on a curving metallic surface, phenomena of twisting or curving will happen to it, this characteristic could be taken full advantage of to detect the

curving surface, in this way, Hough line algorithm can provide us a valuable tool for the curving surface detection.

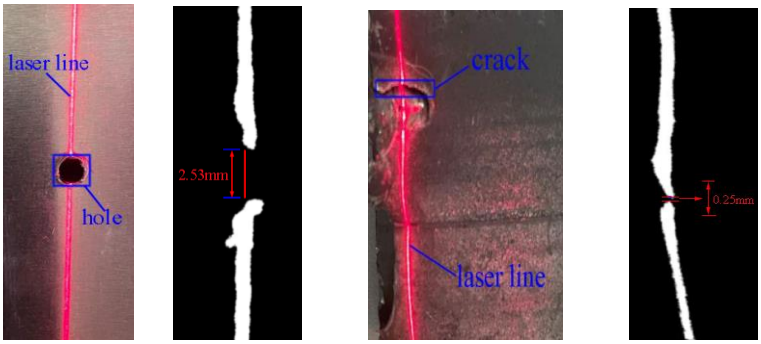

(a) (b) (c) (d)

Fig. 11. A hole detected on metallic surface. ((a): a hole on metallic surface; (b): detection result of the hole in (a) with calculated diameter of 2.53mm; (c): a crack detected on metallic surface; (d): detection result of the crack in (c) with calculated gap of 0.25mm.).

The principle of Hough line detection is shown in Fig.12:

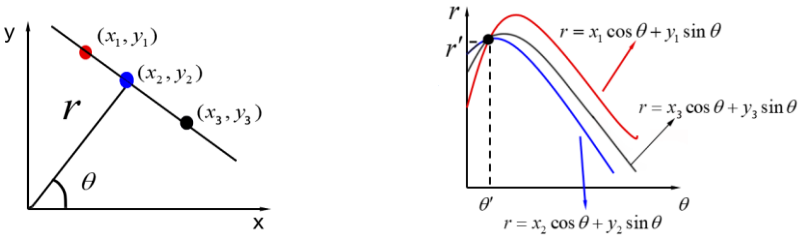

(a): Image space (b): Parametrical polar space

Fig. 12. Transformation from the image space to polar parameter space of Hough line detection.

Here (x_1, y_1) , (x_2, y_2) and (x_3, y_3) are three points on this line in image space, however, in polar parameter space, these three points are expressed as three lines in polar parameter space respectively as following:

$$r = x_1 \cos\theta + y_1 \sin\theta \tag{10}$$

$$r = x_2 \cos\theta + y_2 \sin\theta \tag{11}$$

$$r = x_3 \cos\theta + y_3 \sin\theta \tag{12}$$

The intersection point (r', θ') of above three lines in polar parameter space represents (r, θ) of line in the image space, then lines in image space could be found [10].

Due to the characteristic that laser line will twist or bend when it is reflected on curving surface like Fig.13, we utilize Hough line detection algorithm to inspect curving surface. Fig.13 and Fig.14 demonstrate detection and comparison of flat surface and curved one.

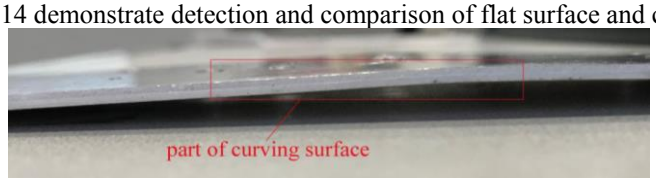

Fig. 13. Surface with curving part.

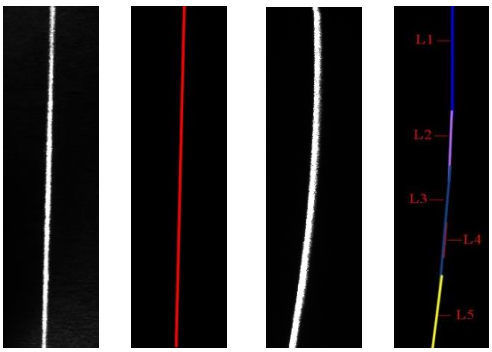

(a) (b) (c) (d)

Fig. 14. Demonstration of curving surface detection using Hough algorithm((a): Laser line reflected on flat surface; (b): Hough line detection on (a); (c): Laser line reflected on curving surface; (d): Hough line detection on (c).).

4 Conclusion

This paper proposes a stereo optical comparison method based on machine vision and laser triangulation for inspection of defects such as holes or cracks on metallic surface, we used stereo cameras with angles calibration facility to alleviate illumination, reflection and laser jitter related problems. In our experiments after a series of image processing methods, we have successfully detected defects, the laser triangulation will be employed for accurate measurement of detected defects. Results from the experiments data confirmed precise detection of defects, position, and sizes. For now, this research is in early step, further studies may require to improve surface detection of metallic surface under different illumination.

References

1. B. Tang, J.Y. Kong, S.Q. Wu, Journal of Image and Graphics, **22**, 1640-1663 (2017)
2. C.X. Wu, B.J. Chen, C.S. Ye. Opt. Laser. Eng, **129** (2020)
3. R. Ranjan, A.R.Khan, C.Parikh, R.Jain, R.P. Mahto, S.Pal, S.K.Pal, D. Chakravarty, J. Manuf. Process, **22**, 237-253 (2016)
4. R. Manish, A.Venkatesh, S. D. Ashok, Mater. Today: Proc, **5**, 12792-12802 (2018)
5. A.S. Nateri, F. Ebrahimi, N. Sadeghzade. Optik (Stuttg.), **125** (2014)
6. Y.C. Sun, Y.J. Pan, Z.X. Bai, Y.L. Wang, Z.W. Lv, Laser Journal, **42**,1-8 (2021)
7. N. Otsu, IEEE Trans. Syst. Man Cybern. **9**, 62-66 (1979)
8. Q. Wang, N. Gui, Y.J. Liu, S.F. Peng, X.T. Yang, J.Y.Tu, S.Y. Jiang, Ann. Nucl. Energy, **148** (2020)
9. W. Rong, Z. Li, W. Zhang, L. Sun, ICMA.2014, 577-582 (2014)
10. D. Bailey, Y. Chang, S.L. Moan, J. Imaging, **6**, 26 (2020).